Vortex Induced Rotation Dynamics of Optical Patterns

V. Caullet, N. Marsal, D. Wolfersberger, and M. Sciamanna

Supélec, OPTEL Research Group, Laboratoire Matériaux Optiques, Photonique et Systèmes (LMOPS), EA-4423, 2 rue Edouard Belin, 57070 Metz, France

(Received 6 March 2012; published 27 June 2012)

We demonstrate that modulation instability leading to optical pattern formation can arise by using nonconventional counterpropagating beams carrying an orbital angular momentum (optical vortices). Such a vortex beam is injected into a nonlinear single feedback system. We evidence different complex patterns with peculiar phase singularities and rotating dynamics. We prove that the dynamics is induced by the vortex angular momentum and the rotation velocity depends nonlinearly on both the vortex topological charge and the intensity of the input beam.

DOI: 10.1103/PhysRevLett.108.263903 PACS numbers: 42.65.Sf, 05.45.−a, 45.70.Qj

Photon orbital angular momentum has been a subject of growing interest. A beam carrying such a momentum, called an optical vortex, has a helicoidal wave front and a ring-shaped intensity profile [1] (Fig. 1). The electric field of such a beam can be written in cylindrical coordinates as $\mathbf{E}(r, \theta, z) = \mathbf{u}(r, z)e^{ic\theta}e^{-ikz}$. $\mathbf{k} = k\hat{z}$ is the wave vector and c is an integer called the topological charge indicating phase fronts which are c intertwined helical surfaces. The orbital angular momentum carried by each of the beam photons is equal to $c\hbar$. Contrary to the spin angular momentum associated with the polarization structure of the light, the orbital angular momentum relies on the photon phase property. Therefore, optical vortices are of both fundamental and application interest. For example, such beams are used as "optical tweezers" or actuators in biophysics [2], micromechanics, and microfluidics [3], or for extra solar planet detection [4]. In optics, propagation of vortices in nonlinear materials shows many interesting phenomena such as frequency conversion [5], wave mixing [6], beams' self-trapping, or peculiar instabilities: spiraling multipoles and azimuthons [7]. While propagating through a nonlinear medium, a common laser beam may also become unstable against a mechanism called modulation instability. This later develops at a characteristic transverse length, resulting in the appearance of correlated satellite beams (pattern) that grow in preferential directions. Such a self-organization process is commonly studied using broad co-(counter)propagating Gaussian beams with wave mixing achieved in either cavity [8–11] or single feedback systems [12–16]. Because of unavoidable or voluntary misalignments in optical experiments, pattern formation is usually accompanied by convective drifting dynamics resulting from a nonlocal coupling between the propagating beams [17–19]. Pattern-forming optical systems may also show phase singularities in the transition to space time chaos [20]. Nevertheless, the effect of a singular beam instead of a nonsingular one as the input pump of a pattern-forming system remains unexplored.

In this Letter, we force our nonlinear single feedback experiment with an optical vortex and show nontrivial pattern dynamics. Complex rotating hexagonal patterns with phase singularities in the satellite beams are evidenced in good qualitative agreement with recent numerical predictions [21]. Contrary to dynamics sustained by noise observed in convective regimes [17,18], we prove that the dynamics is here induced by the vortex orbital angular momentum.

Our demonstration is based on the experiment depicted in Fig. 1. It consists of a photorefractive cobalt doped barium titanate crystal ($BaTiO_3$:Co, $6 \times 6 \times 6$ mm^3) in a single feedback configuration. The lens L_1 imposes the input beam size. The feedback mirror, placed behind the lens L_2, can be precisely moved longitudinally to vary the position of the corresponding virtual mirror (VM) created by the $2f$:$2f$ imaging system (Fig. 1). This allows adjustment of positive (mirror outside the medium) or negative (mirror inside the medium) effective diffraction lengths [22]. We limit our study to the case where the VM is placed at the back face of the crystal. The crystal is

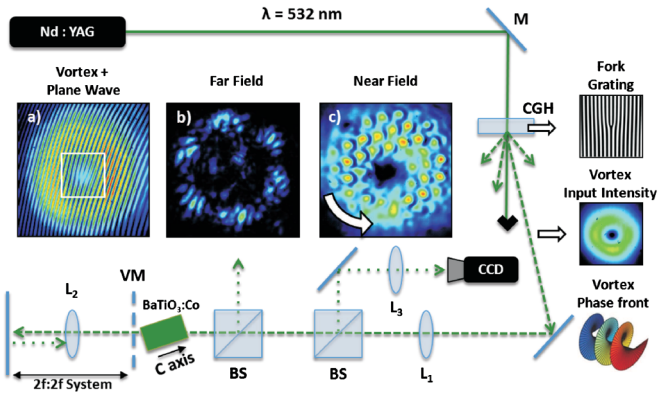

FIG. 1 (color online). Experimental setup. Computer generated hologram (CGH) printed on glass. (a) Interference picture between a vortex beam and a plane wave. (b) Far-field pattern obtained by linear diffraction after a beam splitter (BS) and corresponding to the Fourier transform of the near field observed on picture (c). In picture (b), the central spot has been removed to emphasize the satellite beams.

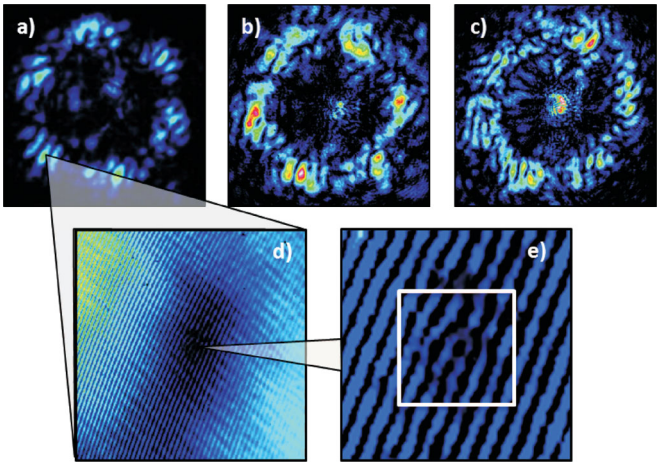

FIG. 2 (color online). (a)–(c) Far-field patterns obtained with different vortex topological charges $c = 1$, $c = 2$, and $c = 3$, respectively. (d)–(e) Zoom on the interference pattern between a part of the satellite beams and a plane wave. A first-order dislocation is visible inside the white square (e).

oriented to provide strong energy coupling between the two counterpropagating beams. The angle between the spontaneous polarization $\hat{c}$ axis of the $BaTiO_3$: Co crystal and the optical axis of the system is set to approximately 25°. For this orientation of the crystal, the large electro-optic coefficient r_{22} gives a strong contribution to the photorefractive response, leading to a two-wave mixing amplification in backward direction [23]. A continuous frequency-doubled Nd:YAG laser emitting at 532 nm is used as the coherent light source. To generate an optical vortex, the laser beam is sent through a transmission grating with a fork-shaped geometry (Fig. 1). Depending on the number of dislocations in the mask, vortices of different topological charges can be selected in the diffraction orders [24]. Finally, the observation of the far and corresponding near field is realized by projecting the backward beam, after passage through the crystal, on a CCD camera.

First, we consider the situation where the system is driven by a conventional Gaussian beam ($c = 0$). Such an experimental configuration has already proved its capacity to generate light self-organization due to modulation instability [16]. Depending on the distance of mirror-crystal and above a certain intensity threshold, a large number of unstable pattern modes can be formed but only a few of them are selected such as stripes or hexagons. The pattern selection intrinsically implies a spontaneous breaking of the translation and rotation symmetry in the system. By varying the feedback mirror tilt angle, an additional breaking of the reflection symmetry gives rise to various pattern geometries. The new pattern modes are usually accompanied by an advectionlike effect giving rise to convective instabilities sustained by noise [19].

The scenario changes when counterpropagating Gaussian beams are substituted by vortices. We first inject a $c = +1$ vortex beam. To test the vortex topological charge, thus the efficiency of the fork grating, we temporarily remove the feedback mirror and monitor the interference pattern composed by the first diffraction order of the grating and a plane wave. The resulting dislocation in the center of Fig. 1(a) indicates a $c = +1$ vortex beam. Second- or third-order dislocations are observed for corresponding higher $c = +2$, $c = +3$. For negative topological charges, a forklike interference pattern similar to Fig. 1(a) is observed but in the opposite direction.

The first example of vortex induced pattern formation is the one shown in Figs. 1(b) and 1(c). The feedback mirror is placed at the back face of the crystal and the intensity of the focused vortex beam can be set from 1 to 100 W/cm^2. For an intensity close to 10 W/cm^2, modulation instability occurs and the system bifurcates to a dynamic pattern state. As for the Gaussian case, we measure an angle $\theta \approx 1°$ between the central spot of the backward beam and the emerged satellite beams, consistent with previous observations [13]. The pattern of near-field intensity distribution looks like a honeycomb structure inside the vortex ring [Fig. 1(c)]. The white arrow indicates a rotating dynamics around the dark center where no instability pops up. The corresponding far field shows complex satellite beams belonging to a circle of instabilities where black lines are visible on top of the satellites [Fig. 1(b)]. A close inspection of the far field indicates the presence of dislocations. Figures 2(a)–2(c) represent the far-field patterns for three different vortex topological charges. The interferogram between one of the satellites and a plane wave is shown on Figs. 2(d) and 2(e). The zoom on Fig. 2(e) illustrates a first-order dislocation indicating the presence of $c = 1$ vortices in the satellites of the far-field pattern. By injecting vortices with higher topological charges ($c = 2$, $c = 3$), far-field patterns become more complex [Figs. 2(b) and 2(c)] as predicted in [21] and whatever the input charge is, the satellite beams are all composed by charge 1 vortices. Closely linked to what we observed but in a different context of beam propagation, similar results occur in anisotropic nonlinear media where the propagation of a vortex with a high topological charge may decay in several first-order vortices [25].

Although the structure of the satellite beams is not affected by the vortex topological charge, the dynamics of the near-field pattern changes drastically. Figure 3 displays a rotating dynamics for two different input vortices: $c = +1$ and $c = -3$. The beam waist of the first vortex ($c = 1$) is equal to 290 μm. The second one ($c = -3$) is equal to 340 μm. The values correspond to measurements realized by the "knife-edge" technique [27]. The time difference between two consecutive images is equal to 0.6 sec. Independent of the different topological charges, we first notice that the near-field patterns do not differ. We identify a honeycomblike self-organization similar to classical hexagonal pattern observed in experiments with counterpropagating Gaussian beams [13,16]. Nevertheless, the pattern is here accompanied by a rotating dynamics

depending on the sign of the topological charge. For positive charges [$c = +1$, Figs. 3(a)–3(d)], the sense of rotation is counterclockwise and clockwise for negative values [$c = -3$, Figs. 3(e)–3(h)]. Contrary to common advection-like effect imposed by a nonlocal coupling of the counter-propagating beams [17,18], the rotating dynamics is here induced by the intrinsic orbital angular momentum of the vortex. Similar results are obtained for pairs of opposite topological charges ($c = \pm 1$, $c = \pm 2$, $c = \pm 3$).

By knowing the time separation between two consecutive pictures, the distance travelled by one spot (red squares in Fig. 3) and the radius of the vortex, one can calculate the linear and angular velocities of the rotation. For $c = 1$, the angular velocity is $\upsilon \simeq 0.15$ rad/s and for $c = -3$ it is $\upsilon \simeq 0.17$ rad/s. These results suggest that the rotation velocity depends on the vortex topological charge. Furthermore, it is worth mentioning that due to photorefractive effect, the input beam intensity influences both the gain and the response time of the two-wave mixing interaction geometry in the crystal [28] and might also have impact on the pattern velocity. All these results are presented in Fig. 4. We study for different topological charges ($c = 1, 2, 3$) the dependency of the pattern near-field angular velocity versus the input beam intensity. For fruitful comparisons, the power and the beam waist of the different vortices have been adjusted to have the same intensity at the input face of the crystal. First, we see that all the curves start at the same input intensity equal to 10 W/cm^2. Below this threshold value, it is difficult to clearly identify a pattern state and therefore impossible to measure a rotation velocity. Second, we observe that the velocity grows with the input intensity. For $c = 1$ the velocity increases from 0.10 to 0.17 rad/s, $c = 2$ from 0.12 to 0.20 rad/s, and $c = 3$ from 0.12 to 0.21 rad/s. These results seem consistent with the fact that, as already mentioned, the increase of the input intensity leads to a faster response time of the photorefractive effect. The corresponding mean linear velocity is of tens of micrometers per second, which corresponds to the relatively slow time response of the photorefractive barium titanate crystal that is of the order of second. A saturation effect appears for intensities above 25 W/cm^2 and is more pronounced for higher charges $c = 2$ and $c = 3$ (Fig. 4). This effect could be linked to the saturation property of the photorefractive nonlinearity [29]. Finally, one can notice that the pattern velocity increases nonlinearly with the topological charge. For an input intensity equal to 20 W/cm^2 (below the saturation effect), the velocity increases from 0.15 rad/s for $c = 1$ to 0.17 rad/s for $c = 2$ and $c = 3$. These velocities correspond respectively to rotation periods of 43 sec for $c = 1$ and 36 sec for $c = 2$ and $c = 3$. The increasing values of the velocity versus the topological charges stem from the linear definition of the vortex orbital angular momentum: the higher c is, the faster the vortex energy flow runs. However, the nonlinear evolution may derive from the interplay between the vortex orbital angular momentum and the nonlinear mechanism of modulation instability. All these observations demonstrate that the rotation velocity depends nonlinearly not only on the input intensity but also on the vortex topological charge. These results should be compared with our previous theoretical study [21]. Although our model does not account for many of the experimental complexities (in particular, the intensity dependency), theory and experiment agree qualitatively on the facts that the mean rotation period ranges from 10 to 100 times the photorefractive time constant and the rotation period varies nonlinearly with c, although the difference remains small (max 15%).

In summary, we have shown experimentally that the peculiar transverse phase property of a vortex beam induces new interesting phenomena in a pattern-forming system. We investigated a photorefractive single feedback experiment where a vortex beam was used as the input beam. Above a certain intensity threshold, modulation

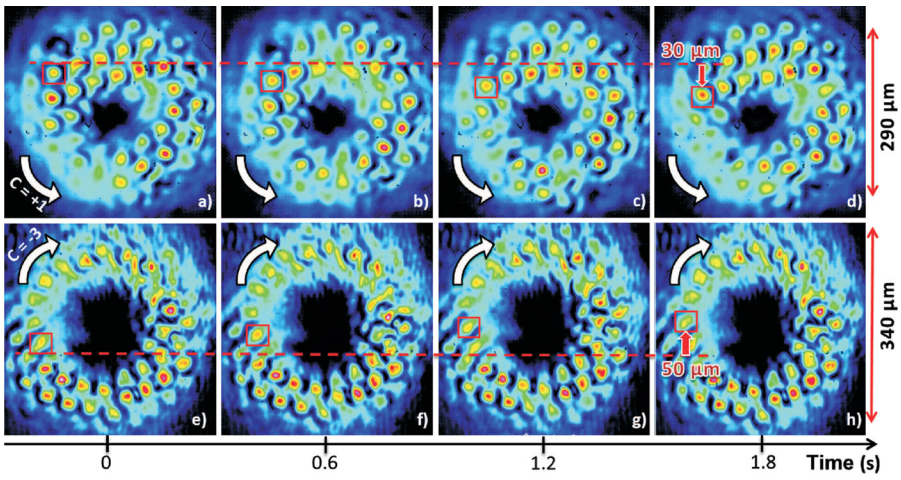

FIG. 3 (color online). Rotation dynamics of the near-field pattern over time for an intensity of the input beams equal to 20 W/cm^2 at the crystal input face. First line (a)–(d): $c = +1$. Second line (e)–(h): $c = -3$. The vertical arrows (d),(h) indicate the direction of motion of one spot located in the red square. The white arrows show the global counter or clockwise rotation of the pattern [26].

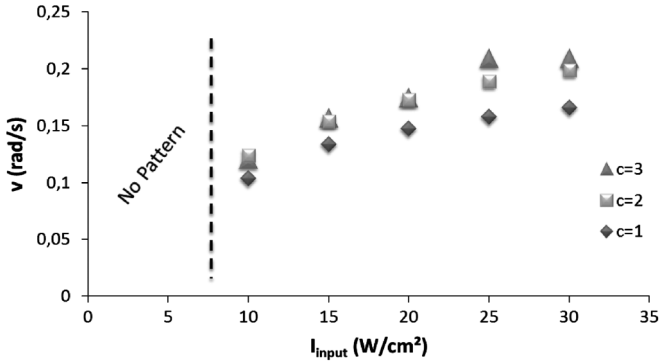

FIG. 4. Near-field pattern velocity for different topological charges c and different input beam intensities.

instability occurs and honeycomb patterns arise in near field. The self-organization is accompanied by a rotating dynamics of a few tens of micrometers per second around the dark center. The sense of rotation depends on the sign of the topological charge and the rotation velocity grows nonlinearly with both the vortex charge and the input beam intensity. Contrary to convective dynamics sustained by noise, the dynamics is here induced by the vortex orbital angular momentum. Finally we noticed that whatever the vortex topological charge is, the corresponding far-field patterns display complex distributed satellite beams with first-order phase dislocations. In a more general context of pattern formation, this result suggests that the geometry of the pattern components depends strongly on the input beam profile.

From the fundamental side, an extension of this work might be the study of the interplay between convective dynamics produced by an intentional nonlocal coupling between two counterpropagating vortices and a rotating dynamics induced by the vortex orbital angular momentum. An other interesting issue is the management of the individual components of the rotating pattern. This could lead, similar to the manipulation of drifting cavity solitons [30], to innovations towards optical buffers and delay lines applications.

The authors acknowledge the support of the Conseil Régional de Lorraine, the Fondation Supélec, the Institut Carnot C3S "Centrale-Supélec Sciences des Systèmes."

[1] G. Molina-Terriza, J. P. Torres, and L. Torner, Nature Phys. **3**, 305 (2007).
[2] J. E. Curtis, B. A. Koss, and D. G. Grier, Opt. Commun. **207**, 169 (2002).
[3] M. E. J. Friese, H. Rubinsztein-Dunlop, J. Gold, P. Hagberg, and D. Hanstorp, Appl. Phys. Lett. **78**, 547 (2001).
[4] J. H. Lee, G. Foo, E. G. Johnson, and G. A. Swartzlander, Phys. Rev. Lett. **97**, 053901 (2006).
[5] K. Dholakia, N. B. Simpson, M. J. Padgett, and L. Allen, Phys. Rev. A **54**, R3742 (1996).
[6] F. Lenzini, S. Residori, F. T. Arecchi, and U. Bortolozzo, Phys. Rev. A **84**, 061801(R) (2011).
[7] A. S. Desyatnikov, L. Torner, and Y. S. Kivshar, Prog. Opt. **47**, 291 (2005).
[8] M. Saffman, D. Montgomery, and D. Z. Anderson, Opt. Lett. **19**, 518 (1994).
[9] D. Kip, M. Soljacic, M. Segev, E. Eugenieva, and D. N. Christodoulides, Science **290**, 495 (2000).
[10] R. Kuszelewicz, I. Ganne, I. Sagnes, G. Slekys, and M. Brambilla, Phys. Rev. Lett. **84**, 6006 (2000).
[11] U. Bortolozzo, A. Montina, F. T. Arecchi, J. P. Huignard, and S. Residori, Phys. Rev. Lett. **99**, 023901 (2007).
[12] G. D'Alessandro and W. J. Firth, Phys. Rev. Lett. **66**, 2597 (1991).
[13] T. Honda, Opt. Lett. **18**, 598 (1993).
[14] G. D'Alessandro, E. Pampaloni, P.-L. Ramazza, S. Residori, and F. T. Arecchi, Phys. Rev. A **52**, 4176 (1995).
[15] S. Residori, Phys. Rep. **416**, 201 (2005).
[16] N. Marsal, D. Wolfersberger, M. Sciamanna, G. Montemezzani, and D. N. Neshev, Opt. Lett. **33**, 2509 (2008).
[17] E. Louvergneaux, C. Szwaj, G. Agez, P. Glorieux, and M. Taki, Phys. Rev. Lett. **92**, 043901 (2004).
[18] F. Papoff and R. Zambrini, Phys. Rev. Lett. **94**, 243903 (2005).
[19] N. Marsal, D. Wolfersberger, M. Sciamanna, and G. Montemezzani, Phys. Rev. A **81**, 031804(R) (2010).
[20] P. Coullet, L. Gil, and J. Lega, Phys. Rev. Lett. **62**, 1619 (1989).
[21] V. Caullet, N. Marsal, D. Wolfersberger, and M. Sciamanna, Opt. Lett. **36**, 2815 (2011).
[22] S. J. Jensen, M. Schwab, and C. Denz, Phys. Rev. Lett. **81**, 1614 (1998).
[23] G. Montemezzani, Phys. Rev. A **62**, 053803 (2000).
[24] V. Y. Bazhenov, M. V. Vasnetsov, and M. S. Soskin, JETP Lett. **52**, 429 (1990).
[25] A. V. Mamaev, M. Saffman, and A. A. Zozulya, Phys. Rev. Lett. **78**, 2108 (1997).
[26] A video is available at http://www.metz.supelec.fr/metz/recherche/optel/images/May2012_vortex.avi
[27] A. E. Siegman, M. W. Sasnett, and T. F. Johnston, IEEE J. Quantum Electron. **27**, 1098 (1991).
[28] S. G. Odoulov, M. Yu. Goulkov, and O. A. Shinkarenko, Phys. Rev. Lett. **83**, 3637 (1999).
[29] N. V. Kukhtarev, V. B. Markov, S. G. Odulov, M. S. Soskin, and V. L. Vinetskii, Ferroelectrics **22**, 949 (1978).
[30] F. Pedaci *et al.*, Appl. Phys. Lett. **92**, 011101 (2008).